# OPTIMIZATION OF WINDING CONDITIONS FOR PREVENTING ROLL DEFECTS CAUSED BY THERMAL-VISCOELASTIC PROPERTY AND EXPERIMENTAL VERIFICATION

**By**

**Hiromu Hashimoto**
**Tokai University**
**JAPAN**

## ABSTRACT

Plastic films are used in many high functional products. They are produced on roll to roll system. The films are continuously wound in the shape of roll using this system. The wound roll is shipped to the store and transportation, in some cases, heat-treated under the various temperatures. Then internal stress of wound roll will be changed due to thermal strain and viscoelastic properties over time. Those factors causes to wound roll defects such as slippage or wrinkling. This paper describes optimization method of winding tension for preventing the wound roll defects by thermo-viscoelastic property based on the optimum design technique. As a result, the optimized tension is confirmed experimentally that the internal stress distributions are very much improved for preventing both wrinkling and slippage.

## NOMENCLATURE

| | | |
|---|---|---|
| $a_T(T)$ | : | time shift factor based on reference temperature |
| $a_T(\sigma)$ | : | time shift factor based on reference stress |
| $c$ | : | specific heat J/(kg･K) |
| $E$ | : | Young's modulus Pa |
| $F$ | : | friction force N |
| $h$ | : | film thickness |
| $k$ | : | thermal conductivity W/(m･K) |
| $L$ | : | nip load N/m |
| $J(t)$ | : | creep compliance $Pa^{-1}$ |
| $r$ | : | roll radius m |
| $r_{out}$ | : | outermost radius m |
| $R$ | : | universal gas constant $8.134\times10^{-3}$ kJ/(K･mol) |
| $t$ | : | time sec |

| | | |
|---|---|---|
| $t'$ | : | reduced time sec |
| $t''$ | : | composite reduced time sec |
| $T$ | : | temperature ℃ |
| $T_0$ | : | initial temperature ℃ |
| $T_\infty$ | : | atmospheric temperature ℃ |
| $\Delta T$ | : | temperature change after wound ℃ |
| $T_w$ | : | winding tension N/m |
| $u$ | : | displacement m |
| $\alpha$ | : | linear thermal expansion coefficient $℃^{-1}$ |
| $\varepsilon$ | : | strain |
| $\nu$ | : | Poisson's ratio |
| $\rho$ | : | density $kg/m^3$ |
| $\sigma$ | : | stress Pa |
| $\sigma_0$ | : | reference stress Pa |
| $\Delta\sigma$ | : | stress increment Pa |
| $\tau$ | : | delay time sec |

**Subscripts**

| | | |
|---|---|---|
| $c$ | : | refer to core |
| $cr$ | : | refer to critical value |
| $f$ | : | refer to film |
| $r$ | : | refer to radial direction |
| $\theta$ | : | refer to tangential direction |

## INTRODUCTION

Plastics films are used in many products to high functionality flexible devices such as optical film, lithium-ion secondary battery and fuel-cell stack. Recently, increase in demand of the products is expected because of increasing electronic devices and fuel cell vehicle. The devices have being manufactured by roll to roll system. In this system, the films are finally wound in the shape of roll [2]-[4]. The wound roll is shipped to the store and transportation, in some cases, heat-treated under the various temperatures. Then internal stress of wound roll will be changed due to thermal strain and viscoelastic properties over time [5]-[6]. As a result, those factors causes to wound roll defects such as slippage and wrinkling. For the problem, viscoelastic model of internal stress of wound roll was presented [7]. On the other hand, in our past study, the optimization method of winding tension was proposed for preventing roll defects [1]. However, the papers considered the thermo-viscoelastic property are very few. Therefore, this paper describes optimization method of winding tension and for preventing the wound roll defects by thermo-viscoelastic property.

Before considering the thermo-viscoelastic property, the creep compliance change was measured by compression/tensile creep tests under various load stress and temperature conditions to investigate the creep behavior of a polypropylene film as test film under the conditions, winding tension $T_w$ = 100 [N/m], nip load $L$ = 235 [N/m] and ambient temperature change after wound $\Delta T$ = 10 [K]. From the experimental results, magnitude of the change was affected by these conditions. In order to apply the effect into winding model, an empirical formula was obtained based on the experimental results. It is possible to estimate the creep compliance values on arbitrary

stress/temperature condition and was expressed by generalized Voigt model. The predicted values generally correspond to the experimental values. In the present optimization method, the wind-up tension was gradually changed in the radial direction to minimize the tangential stresses under the constraint of nonnegative tangential stresses. At the same time, we considered the friction conditions to prevent the slippage between web layers due to a decrease of radial stresses and friction force.

To confirm the effectiveness of optimization, the internal stress of wound roll was measured on the above conditions. Moreover, impact experiment was carried out whether wound roll has suitable friction force for preventing the slippage.

As a result of optimization, the wind-up tension was gradually decreased in the radial direction, and was finally significantly increased. This is because of preventing the slippage and winkling simultaneously. Moreover, it was confirmed that theoretical results showed in fairly good agreement with the experimental results. From the impact experiment, it was found that there is no risk of occurring the slippage in the case of optimal tension, whereas the slippage was occurred using the wound roll with taper tension.

## INTERNAL STRESS ANALYSIS MODEL

### Modeling

In Fig. 1, the equilibrium equation for internal roll stress and the compatibility condition equation for strain are given as

$$r\frac{\partial \sigma_r}{\partial r} + \sigma_r - \sigma_\theta = 0 \qquad \{1\}$$

$$r\frac{\partial \varepsilon_r}{\partial r} + \varepsilon_\theta - \varepsilon_r = 0 \qquad \{2\}$$

where $\sigma_r$, $\sigma_\theta$, $\varepsilon_r$, $\varepsilon_\theta$, $r$ indicate radial and circumferential internal stress, strain in radial and circumferential directions, radial position of wound roll, respectively.

Moreover, given the assumption which web is linear viscoelastic body, the relational expressions of strain and stress in radial and circumferential direction after wound up are expressed as;

$$\varepsilon_r(t) = \int_{t_s}^{t}\left[ J_r(t-\tau')\frac{\partial \sigma_r(\tau')}{\partial \tau'} + J_{r\theta}(t-\tau')\frac{\partial \sigma_\theta(\tau')}{\partial \tau'} + \frac{\partial\left(\alpha_r\left(T_f(\tau')\right)\Delta T_f(\tau')\right)}{\partial \tau'}\right] d\tau' \qquad \{3\}$$

$$\varepsilon_\theta(t) = \int_{t_s}^{t}\left[ J_\theta(t-\tau')\frac{\partial \sigma_\theta(\tau')}{\partial \tau'} + J_{\theta r}(t-\tau')\frac{\partial \sigma_r(\tau')}{\partial \tau'} + \frac{\partial\left(\alpha_\theta\left(T_f(\tau')\right)\Delta T_f(\tau')\right)}{\partial \tau'}\right] d\tau' \qquad \{4\}$$

In these equations, thermal strain is considered in the third term on the right side, $\alpha$ is the linear expansion coefficient, $T_f$ represents the temperature of the wound roll.

On the other hand, creep function $J(t)$ in the generalized Voigt model as shown in Fig. 2 is expressed as

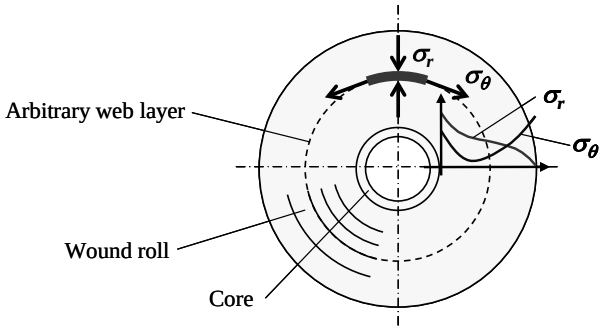


Figure 1－Radial stress and circumferential stress within wound roll

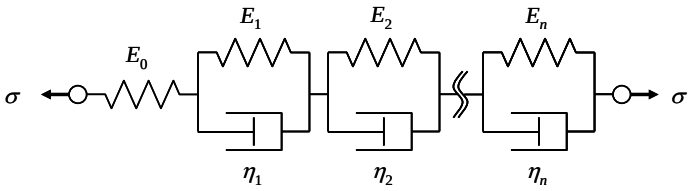


Figure 2－Generalized Voigt model

$$J(t) = J_0 + \sum_{i=1}^{n} J_i\left(1 - e^{-t''/\tau_i}\right) \qquad \{5\}$$

Substituting Eqs. {3}, {4} into Eqs. {1}, {2}, the governing equation for internal stress of wound roll considering thermo-viscoelastic property can be obtained as follows;

$$\int_{t_s}^{t} \left\{ \begin{array}{l} J_\theta(t-\tau')\dfrac{\partial}{\partial\tau'}\left(r^2\dfrac{\partial^2\sigma_r(\tau')}{\partial r^2}\right) \\ +\left[r\dfrac{\partial J_\theta(t-\tau')}{\partial r}+3J_\theta(t-\tau')\right]\dfrac{\partial}{\partial\tau'}\left(r\dfrac{\partial\sigma_r(\tau')}{\partial r}\right) \\ +\left[r\dfrac{\partial J_\theta(t-\tau')}{\partial r}+J_\theta(t-\tau')-J_r(t-\tau')\right]\dfrac{\partial\sigma_r(\tau')}{\partial\tau'} \\ +\dfrac{\partial}{\partial\tau'}\left[r\dfrac{\partial\left(\alpha_\theta\left(T_f(\tau')\right)\Delta T_f(\tau')\right)}{\partial r}\right] \\ +\dfrac{\partial\left(\left(\alpha_\theta\left(T_f(\tau')\right)-\alpha_r\left(T_f(\tau')\right)\right)\Delta T_f(\tau')\right)}{\partial\tau'} \end{array} \right\} d\tau' = 0 \qquad \{6\}$$

To predict the radial stress while changing time and temperature of wound roll, Eq. {6} is discretized with respect to time under the two boundary conditions listed below.

$$\frac{u(t)_{r=r_C}}{r_C} = \frac{\sigma_r(t)}{E_C}\bigg|_{r=r_C} + \int\left(\alpha_C\frac{\partial\Delta T_C(\tau')}{\partial\tau'}\right)d\tau' = \varepsilon_\theta(t)\big|_{r=r_C} \qquad \{7\}$$

$$\Delta\sigma_r(t)\big|_{r=r_{out}} = 0 \qquad \{8\}$$

where $E_c$ , $\alpha_c$, $t_0$ indicate the elastic modulus of the core, the linear expansion coefficient of the core and winding start time.

On the other hand, temperature in the wound roll is calculated from the following unsteady heat conduction equation.

$$\frac{1}{r}\frac{\partial}{\partial r}\left(kr\frac{\partial T}{\partial r}\right) = \rho c\frac{\partial T}{\partial t} \qquad \{9\}$$

The boundary conditions at the outermost and innermost layers are given respectively as,

$$-k_f\frac{\partial T_f(t)}{\partial r}\bigg|_{r=r_{out}} = \kappa\big|_{r=r_{out}}\left(T_f(t)\big|_{r=r_{out}} - T_\infty\right) \qquad \{10\}$$

$$-k_c\frac{\partial T_c(t)}{\partial r}\bigg|_{r=r_c-h_c} = \kappa\big|_{r=r_c-h_c}\left(T_\infty - T_c(t)\big|_{r=r_c-h_c}\right) \qquad \{11\}$$

Moreover, the boundary conditions at the interface between the core and film are as follows.

$$-k_c\frac{\partial T_c(t)}{\partial r}\bigg|_{r=r_c} = -k_f\frac{\partial T_f(t)}{\partial r}\bigg|_{r=r_c} \qquad \{12\}$$

$$T_c(t)\big|_{r=r_c} = T_f(t)\big|_{r=r_c} \qquad \{13\}$$

Solving Eq. {9} with Eqs. {10} to {13} under the initial condition of $T(t_0) = T_0$, the temperature distribution in the wound roll will be determined.

**Creep compliance**

To predict the internal stress of wound roll using the above analysis model, it is necessary to determine the prediction expression of creep compliance. In this study, tensile creep (stress: 2, 4, 6 [MPa], temperature: 23, 31, 40, 50 [℃]) and compression creep (stress: 0.25, 0.5, 1.0, 1.5 [MPa], temperature: 23, 31, 40, 50 [℃]) tests were conducted using polypropylene film under various temperature and applied stress. The creep test conditions are listed in Table 1.

| Testing direction | Compression | Tension |
|---|---|---|
| Load stress $\sigma_L$ [MPa] | 0.25, 0.5, 1, 1.5 | 2, 4, 6 |
| Testing Temperature $T$ [℃] | 23, 31, 40 | 23, 31, 40, 50 |
| Measurement time [hour] | 24 | 3 |
| Strain rate [$sec^{-1}$] | $1.0\times10^{-3}$ | $4.8\times10^{-3}$ |

Table 1 – Creep test conditions

As shown in Fig. 3, the measurement results of creep compliance in circumferential direction strongly depend on temperature. From these results, the master curve of creep compliance in the circumferential direction for reduced time $t'$ is given as Fig. 4. Moreover, stress dependence of time- temperature shift factor is given approximately as shown in Fig. 5.

From Fig. 3, the results of creep compliance also depend on the stress, and the combined master curve of creep compliance for reduced combined time $t''$ is given as Fig. 6. Then, the time-stress shift factor is approximated as shown in Fig. 7.

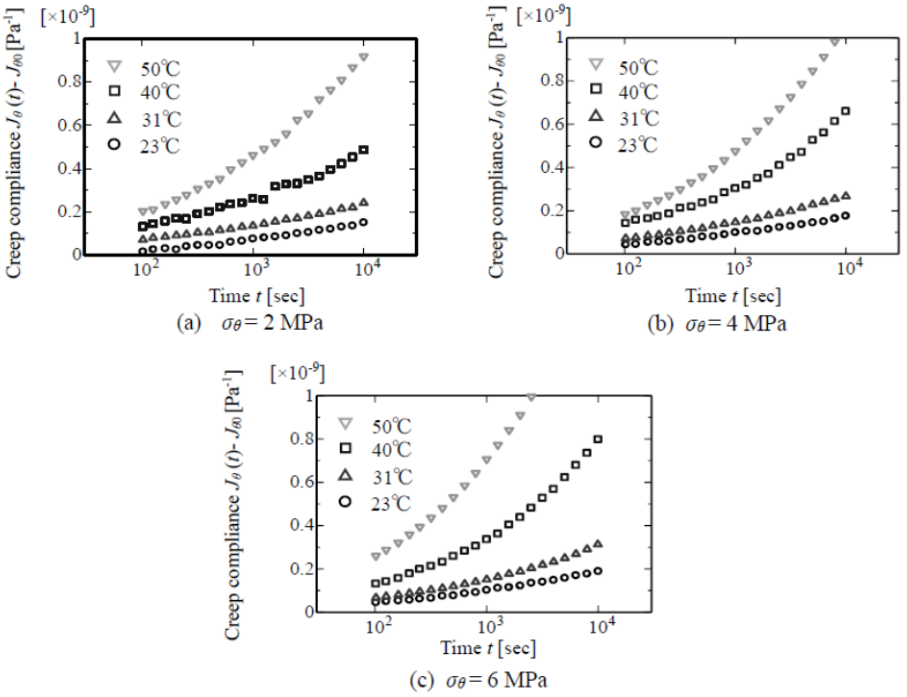


Figure 3－Measurement results of creep compliance in circumferential direction

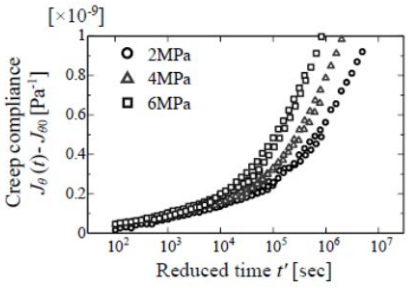


Figure 4－Master curve of creep compliance in circumferential direction

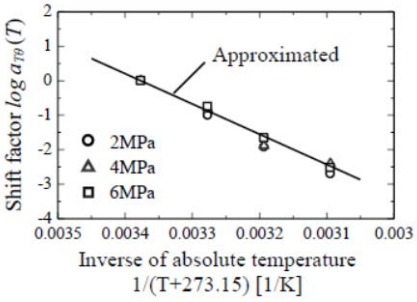


Figure 5－Stress dependence of time-temperature shift factor in circumferential direction

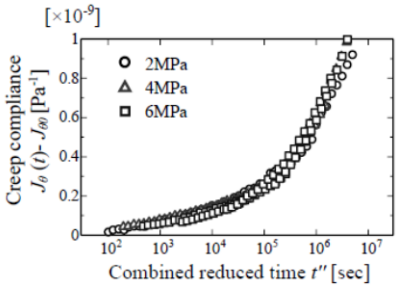


Figure 6—Combined master curve of creep compliance in circumferential direction

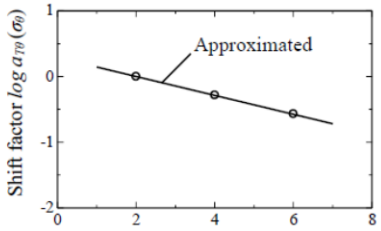


Figure 7 – Time-stress shift factor in circumferential direction

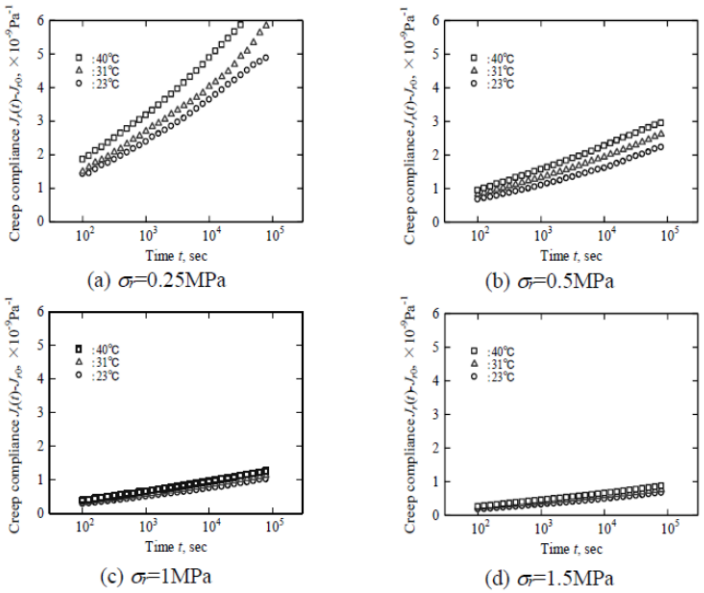


Figure 8 – Measurement values of creep compliance in radial direction (Standard temperature $T_0$=23°C)

Based on the same procedure, the results for the creep function in radial direction are obtained as shown in Fig. 8 to Fig. 11.

In these figures, the reduced and combined reduced time, $t'$ and $t''$, are defined respectively as follows:

$$t' = \frac{t}{a_T(T)} \qquad \{14\}$$

$$t'' = \frac{t'}{a_T(\sigma)} \qquad \{15\}$$

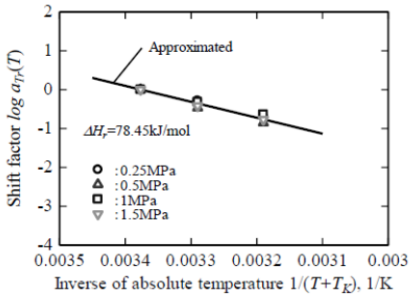


Figure 9 – Time-temperature shift factor in radial direction

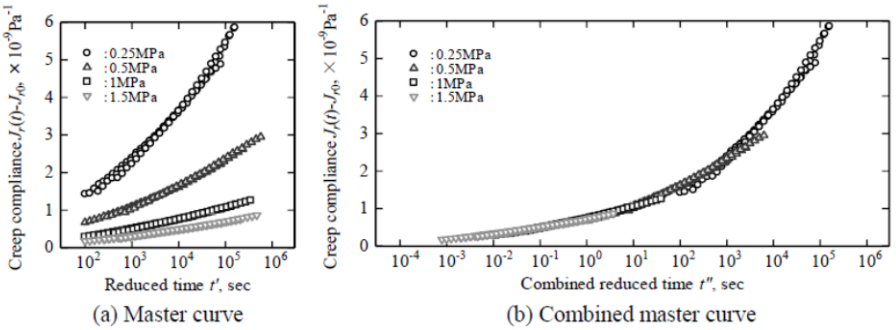


Figure 10 – Combined master curve of creep compliance in radial direction
(Standard radial stress $\sigma_{r0}$=0.25MPa)

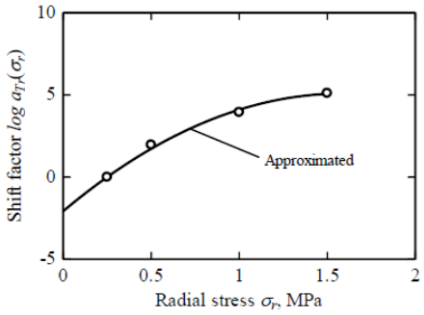


Figure 11 – Time-stress shift factor in radial direction

In which, $T_{\theta 0}$=23 [℃], $\sigma_{\theta 0}$=2.0 [MPa], $T_{r0}$=23 [℃] and $\sigma_{r0}$=2.0 [MPa] were set as reference conditions. As a result, time shift factors of temperature and stress in radial and circumferential directions are given as follow;

$$\log a_{T\theta}(T_f) = \frac{78.36}{2.303R}\left(\frac{1}{T+273.15}-\frac{1}{T_0+273.15}\right) \quad \{16\}$$

$$\log a_{T\theta}(\sigma_\theta) = -1.439\times10^{-7}(\sigma_\theta-\sigma_{\theta 0}) \quad \{17\}$$

$$\log a_{Tr}(T_f) = \frac{164.36}{2.303R}\left(\frac{1}{T+273.15} - \frac{1}{T_0+273.15}\right) \quad \{18\}$$

$$\log a_{Tr}(\sigma_r) = -2.804\times10^{-12}(\sigma_r - \sigma_{r0})^2 + 7.596\times10^{-6}(\sigma_r - \sigma_{r0}) \quad \{19\}$$

where $R$ = 8.134 kJ(K·mol) indicates universal gas constant.

From the tensile and compression creep test, it was confirmed that creep compliance was dependent on temperature and stress, and the prediction expressions of creep compliance in radial and circumferential directions were obtained as follow;

$$\begin{aligned} J_\theta(t) = J_{\theta 0} &+ 5.507\times10^{-11}\left(1-e^{-t^*/2.567\times10^2}\right) + 6.315\times10^{-11}\left(1-e^{-t^*/3.533\times10^3}\right) \\ &+ 7.536\times10^{-11}\left(1-e^{-t^*/3.478\times10^4}\right) + 2.929\times10^{-10}\left(1-e^{-t^*/3.363\times10^5}\right) \\ &+ 1.331\times10^{-9}\left(1-e^{-t^*/6.111\times10^6}\right) \end{aligned} \quad \{20\}$$

$$\begin{aligned} J_r(t) = J_{r0} &+ 3.814\times10^{-10}\left(1-e^{-t^*/2.396\times10^{-3}}\right) + 5.010\times10^{-10}\left(1-e^{-t^*/7.588\times10^{-1}}\right) \\ &+ 9.226\times10^{-10}\left(1-e^{-t^*/6.532\times10^1}\right) + 1.753\times10^{-9}\left(1-e^{-t^*/3.907\times10^3}\right) \\ &+ 3.098\times10^{-9}\left(1-e^{-t^*/1.116\times10^5}\right) \end{aligned} \quad \{21\}$$

**Experimental verification**

To verify the winding analysis model, the radial stress of wound roll and temperature were measured. The experimental apparatus used in the measurement was constructed as the roll-to-roll manufacturing process as shown in Fig. 12, which can control the winding tensions, winding velocity and nip load. Film was transferred from the unwinding to the rewinding through the pinch roller and nip roll, and rewound finally. The radial stress and temperature were measured by using pressure sensor and temperature sensor which were inserted in wound roll as shown in Fig. 13. Furthermore, the temperature around wound roll was changed after winding of web using a chamber as shown in Fig. 14. In this study, the experiment was conducted on the conditions, winding tension $T_w$=100 N/m, nip load $L$=235 N/m and ambient temperature change after wound $\Delta T$=10 K using the polypropylene film.

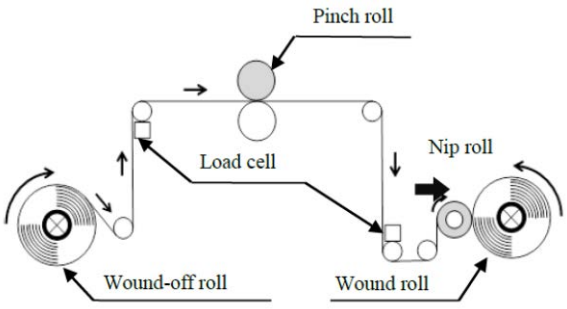


Figure 12 – Experimental apparatus

The physical properties of test film and experimental conditions are listed, respectively, in Table 2 and Table 3.

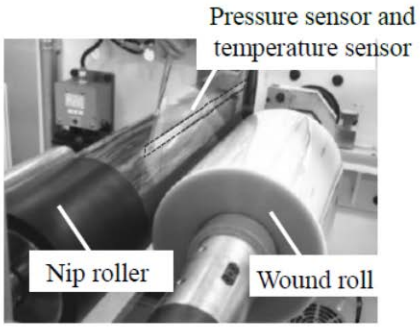


Figure 13－Measuring method of radial stress of a wound roll

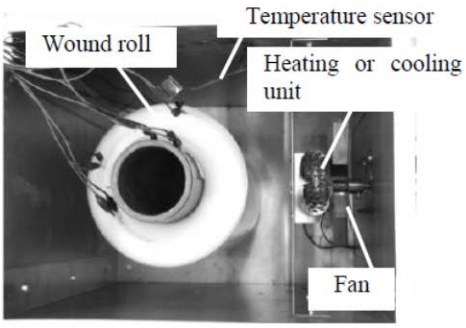


Figure 14 – Storage chamber

| Parameter | Value |
|---|---|
| Material | Polypropylene |
| Thickness $h_f$ [μm] | 48 |
| Composite RMS roughness $R_{ff}$ [μm] | 0.081 |
| Friction coefficient $\mu$ | 0.23 |
| Thermal conductivity $k_f$ [W/(m·K)] | 0.125 |
| Specific heat $c_f$ [J/(kg·K)] | 1650 |
| Density $\rho_f$ [kg/m$^3$] | 906 |

Table 2 – Physical properties of test film

| Parameter | | | Value |
|---|---|---|---|
| Winding velocity $V$ [m/s] | | | 1.0 |
| Winding tension $T_w$ [N/m] | | | 100 |
| Nip load $L$ [N/m] | | | 235 |
| Web width [m] | | | 0.28 |
| Core | Radius $r_c$ [m] | | 0.045 |
| | Thickness $h_c$ [m] | | 0.007 |
| | Young's modulus $E_c$ [Pa] | | $3.0\times10^9$ |
| | Thermal conductivity $k_c$ [W/(m·K)] | | 0.47 |
| | Specific heat $c_c$ [J/(kg·K)] | | 920 |
| | Density $\rho_c$ [kg/m$^3$] | | 1940 |
| | Expansion coefficient $\alpha_c$ [1/K] | | $1.4\times10^{-5}$ |
| Ambient temperature in room $T_{room}$ [℃] | | | 24 |
| Ambient temperature in chamber [℃] | | | 44 |
| Storage time [hour] | | | 24 |
| Heat-transfer coefficient $\kappa$ [W/(m$^2$·K)] | | Inside core | 1.8 |
| | | Outside roll | 33.1 |

Table 3 – Experimental conditions

Figure 15 shows the predicted and measured results of in-roll temperature change. The solid line and plots indicate the predicted and measured values. In this figure, solid lines, plots and error bars show the predicted value, mean value of three measurements and variations, respectively.

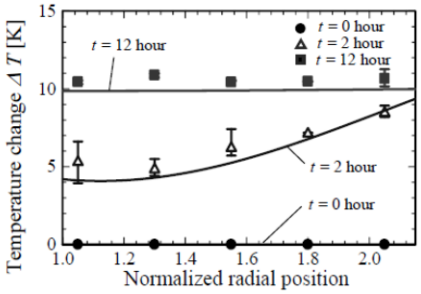


Figure 15 – Predicted and measured results of temperature change

The predicted values of the radial stress distribution indicated that the value largely degrease with over time and the in-roll temperature change, especially adjacent to the core. In addition, the predicted values generally agree with the measured values.

Figure 16 shows the predicted and measured results of radial stress. As shown in this figure, the radial stress of wound roll was momentarily changed similar to results of temperature change in Fig. 15. The reason obtained the results is because creep deformation occurred by stress and in-roll temperature change. It was confirmed that the measured values are relatively in good agreement with the predicted results.

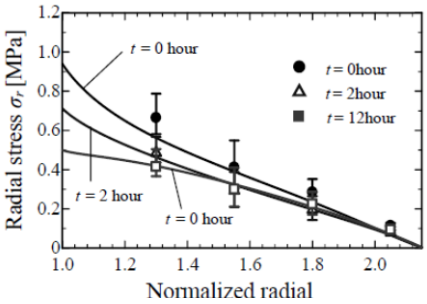


Figure 16 – Predicted and measured results of radial stress

## OPTIMIZATION

### Optimization method

In the present optimization method, the wind-up tension is gradually changed in the radial direction as shown in Fig. 17 to minimize the tangential stresses under the constraint of nonnegative tangential stresses. At the same time, we considered the friction conditions to prevent the slippage between web layers due to a decrease of radial stresses and friction force.

In this study, the design variable vector was set as follows;

$$\boldsymbol{X} = (\Delta T_{w1}, \Delta T_{w2}, \quad \cdots \quad \Delta T_{wm}) \qquad \{22\}$$

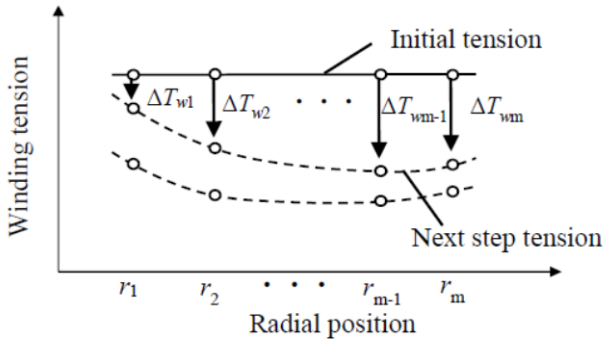


Figure 17 – Evolution of winding tension under optimization process

All of the constraint conditions were summarized as the following inequality expression:

$$g_i(\boldsymbol{X}) \le 0 \quad (i = 1 \sim 20) \tag{23}$$

where the constraint functions in Eq. {23} are defined as follows.

$$\left.\begin{aligned} & g_1 = \Delta T_{w1\min} - \Delta T_{w1}, \quad g_2 = \Delta T_{w2} - \Delta T_{w2\max}, \\ & g_3 = \Delta T_{w3\min} - \Delta T_{w3}, \quad g_4 = \Delta T_{w4} - \Delta T_{w4\max} \\ & \qquad \vdots \qquad\qquad\qquad \vdots \\ & g_{17} = \Delta T_{w17\min} - \Delta T_{w1}, \quad g_{18} = \Delta T_{w18} - \Delta T_{w18\max}, \\ & g_{19} = -\left[\sigma_\theta(t)\right]_{\Delta T_f}, \quad g_{20} = \left[F(t)\right]_{\Delta T_f} - F_{cr} \\ & \qquad\qquad\qquad\qquad\qquad (for\ r \le 0.88 r_{\max}) \end{aligned}\right\} \tag{24}$$

The objective function is expressed as follows:

$$f(\boldsymbol{X}) = \int_{r_c}^{r_{\max}} \left[ \left( \frac{F(r,t)\big|_{t=0}}{F_{cr}} - 1 \right)^2 + \left( \frac{\sigma_\theta(r,t)\big|_{t=0}}{\sigma_{\theta ref}} \right)^2 \right] \mathrm{d}r \tag{25}$$

Then, the optimization problem is described as

$$\text{Find } \boldsymbol{X} \text{ to minimize } f(\boldsymbol{X}) \text{ subjected to } g_i(\boldsymbol{X}) \le 0 \quad (i = 1 \sim 20) \tag{26}$$

The successive quadratic programming, which is a typical mathematical programming method, was used as the optimization technique.

**Result and discussion**

Figure 18 shows the wind-up tension obtained. From the results, the wind-up tension of optimum design was gradually decreased in the radial direction, and was finally significantly increased. This is because of preventing the slippage and winkling simultaneously.

Figure 19 shows results of radial stress and internal stress conditions. In these figures, the solid and dash lines indicate the results of optimized tension and taper tension, and plots indicate the measured results. The radial stress was gradually decreased with time. As can be seen in Figs. 19 (b) and 19(c), the radial stress under the optimized wind-up tension becomes lower and nearly constant for a wide range in the radial direction with a suitable level, and then the circumferential stress becomes zero level but not below zero. This type of circumferential stress distribution has an advantage to prevent both wrinkling and creep simultaneously in the wound roll. In addition, Fig. 19 (d) shows the possibility of preventing the slippage in the wound roll due to the suitable level of friction force more than the critical slippage line. Moreover, to observe the occurrence of slippage, impact test as shown in Fig. 20 was conducted, and in the case of optimized tension, there is no observed the slippage as shown in Fig. 21. As a result, it was confirmed that theoretical results showed in fairly good agreement with the experimental results.

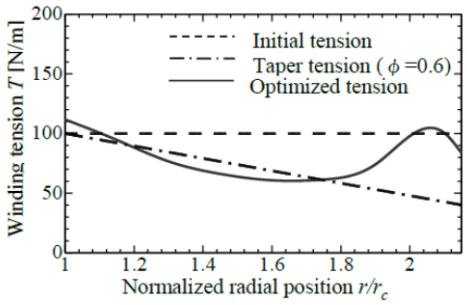


Figure 18 – Result of optimum design

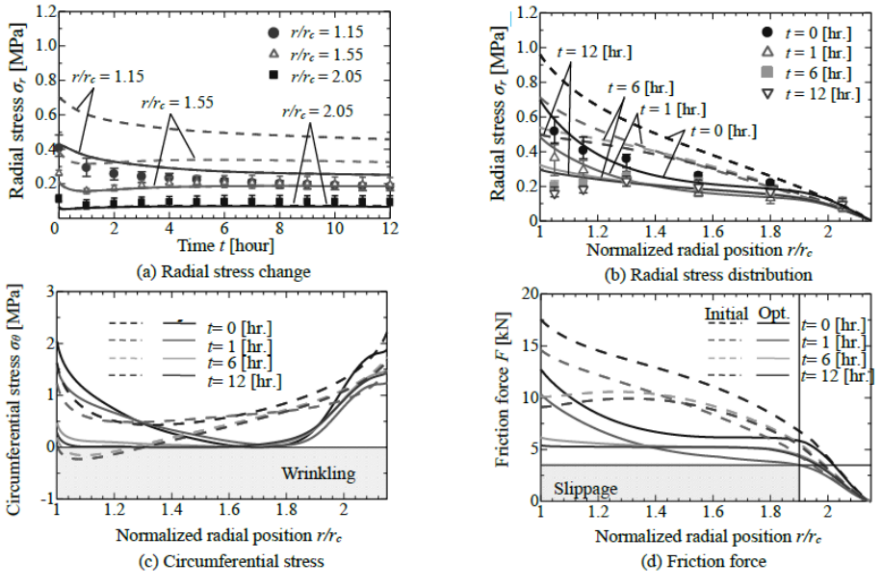


Figure 19 – Optimum solution of tension design considering thermos-viscoelastic property

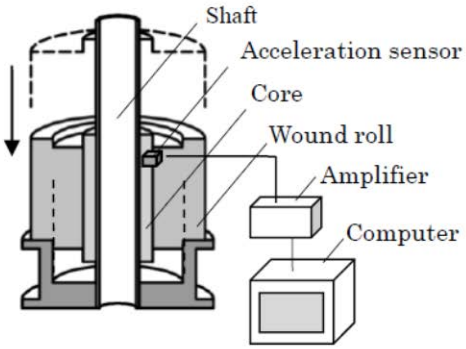


Figure 20－Schematic of impact test in wound roll

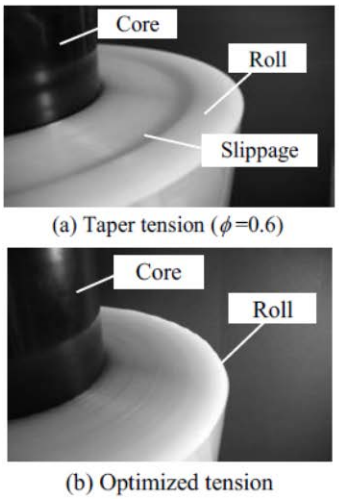


Figure 21 – Slippage observed after impact load test

## CONCLUSIONS

In this study, optimization of winding tension was applied for preventing the wound roll defects by thermo-viscoelastic property. It was verified theoretically and experimentally that the internal stress and friction force distributions in the wound roll are very much improved and it is possible to prevent the wrinkling, creep and slippage effectively.

## REFERENCES

1. Hashimoto, H., Puttha, J., and Mongkol, M., "Optimum Winding Tension and Nip-Load into Wound Webs for Protecting Wrinkles and Slippage," JSME Journal of Advanced Mechanical Design, Systems, and Manufacturing, Vol. 4, No.1, 2010, pp. 214-225.
2. Good, J. K., "The Abilities & Inabilities of Wound Roll Models to Predict Winding Defects," Proceedings of the Eighth International Conference on Web Handling, 2005, pp. 453-523.
3. Hakiel, Z., "Nonlinear Model for Wound Roll Stress," TAPPI Journal, Vol. 70, No. 5 1987, pp. 113-117.
4. Willett, M. S. and Poesch, W. L., "Determining the Stress Distributions in Wound Reels of Magnetic Tape Using a Nonlinear Finite-Difference Approach," ASME Journal of Applied Mechanics, Vol. 55, 1988, pp. 365-371.
5. Qualls, W. R. and Good, J. K., "Thermal Analysis of a Round Roll," ASME Journal of Applied Mechanics, Vol. 64, 1997, pp. 871-876.
6. Lei, H., Cole, K. A. and Weinstein, S.J., "Modeling Air Entrainment and Temperature Effects in Winding," ASME Journal of Applied Mechanics, Vol. 70, 2003, pp. 902-914.
7. Qualls, W. R. and Good, J. K., "An Orthotropic Viscoelastic Winding Model Including a Nonlinear Radial Stiffness," ASME Journal of Applied Mechanics, Vol. 64, No. 1, March, 1997, pp. 201-208.